Mechanical/Environmental Fatigue Transient Effects in AISI 304 Stainless Steel

Y. KATZ, A. BUSSIBA and H. MATHIAS
Nuclear Research Centre-Negev, P.O. Box 9001, Beer-Sheva 84190, Israel

ABSTRACT

Fatigue transient effects have been investigated in AISI 304 metastable austenitic stainless steel. The present experimental study is centered on a combined mechanical/environmental interactive problem including single overload and simultaneous hydrogen charging at 296K. Generally, fracture mechanics methods were applied and analyzed indicating the phenomenological resemblance of the delayed retardation in the environmental affected material as compared to unhydrogenated specimens. Finally, a proposed formulation is discussed in which the mechanical/ environmental interactive effects are expressed by modified values of the nominal overload intensification or level factors.

KEYWORDS

Overload level; fatigue; plastic zone; retardation; crack propagation; affected crack length; effective, constant amplitude, stress intensity range; hydrogenated; interactive effects.

INTRODUCTION

The current experimental study is aimed to elaborate on a mechanical/ environmental interactive problem in fatigued AISI 304 austenitic stainless steel. Particular attention is paid to the additional role of the aggressive environment under complex conditions. The experimental program was actually based on a single overload with subsequent fatigue crack extension in hydrogen environment at 296K.

Previous investigations on steady state fatigue crack growth in AISI 304 (Bussiba et al., 1981) on single overload and fatigue retardation in AISI 304 (Katz et al., 1982, 1984) and on hydrogen effects in AISI 304, 316 and 310 austenitic stainless steels (Mathias et al., 1977, 1978, 1982) provided beneficial background, really essential for the current investigation. While dealing with environmental effects on the steady-state fatigue crack

propagation rate (FCPR), there have been some attempts to adopt superposition or competitive models. In the present situation additional influences of load effects are involved during the sub-critical fatigue growth, which are described and analyzed.

EXPERIMENTAL PROCEDURE

AISI 304 stainless steel was selected with the following chemical composition (in wt/%); Cr-18.6, Ni-9.5, Mn-1.2, Mo-0.23, C-0.05, Si-0.44, Cu-0.25, S-0.016, P-0.033, Fe-bal. Standard mechanical properties were obtained at 296K including measurements of the critical fracture toughness parameters. Fatigue testing was performed by using three-point bending specimens with a span length (S) of 100 mm, thickness (B) of 19 mm and width of 40 mm and initial crack length (a_o) of 21.5 mm. The machined notch was precracked in fatigue with extra care to ensure negligable residual damage at the crack tip vicinity.

For the cyclic loading, a closed-loop electrohydraulic testing machine was utilized. Crack growth was monitored by an electro-potential method after a proper calibration procedure. The entire fatigue run was tracked by an acoustic emission (AE) set-up which provided comparative results for the unhydrogenated (UH) and the hydrogenated (H) specimens. Electrolytic hydrogen charging was performed at room temperature by means of a built-in charging cell, which included a platinum wire as an anode and a 1N H_2SO_4 aqueous solution. The applied current density near the crack region was 10 mA/cm^2. Figure 1 illustrates some details of the experimental set-up.

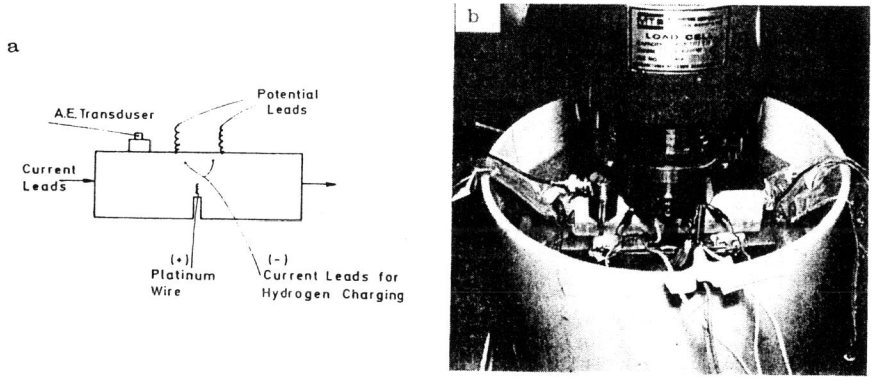

Fig. 1. Experimental set-up; (a) schematic, (b) actual.

Steady state FCPR and single overload retardation behavior were studied. For the UH material the frequency f = 10 Hz was applied with overload levels, $q = \Delta K_{OL}/\Delta K_{CA}$, between 1.35 and 2.50 for $R = K_{min}/K_{max} \simeq 0$. These conditions were also preserved for H specimens, with the addition of frequency effect studies in the range between 1 and 80 Hz. The tests were carried out at a constant stress intensity range ΔK_{CA} by applying a sinusoidal waveform at 296K. The nominal stress intensity amplitude range for the tested specimens was computed according to the following relationship (ASTM E-399, 1987):

$$K = P\ S\ Y\ /(B\ W^{3/2}) \qquad (1)$$

The described procedure established the FCPR vs. ΔK, as well as the FCPR dependency on the applied single overload. Before and after the single overload a constant nominal stress intensity range, ΔK_{CA}, was applied. For the UH material FCPR curves were determined extensively from the near threshold K_{th}, up to the critical upper bound value, ΔK_{Ifc}, described elsewhere (Katz et al., 1981, 1984). Moreover, in addition to the FCPR curves, the retardation behavior in the CTS was studied as well, including its dependency on q and on structural effects. However, for the H material, mainly stage II was experimentally covered.

Finally, fractographic studies were performed. Steady state fatigue fracture modes as well as mode transitions along the overload affected crack length were observed and analyzed, in UH and H specimens. With respect to the latter specimens, particular attention was given to the possible secondary effects due to cathodic charging. Thus, caution was taken in order to avoid post-charging masking of typical features due to cyclic loading, accompanied by the simultaneous cathodic charging.

EXPERIMENTAL RESULTS

The tensile properties at 296K were as follow: yield stress (0.2% offset), 416 MPa; ultimate tensile stress, 660 MPa; elongation, 45 percent. Figure 3 shows the frequency effect on the fatigue crack growth rate in H material. For reference, the stage II region of the FCPR vs. ΔK curve in the UH material is shown for f=10 Hz. As indicated, a narrow discrepancy exists at 10 Hz between the H and UH specimens, actually expected due to the rate dependency of environmental influences. In UH specimens only minor changes were obtained at room temperature, which has been confirmed in cyclic loading along a frequency range of four decades.

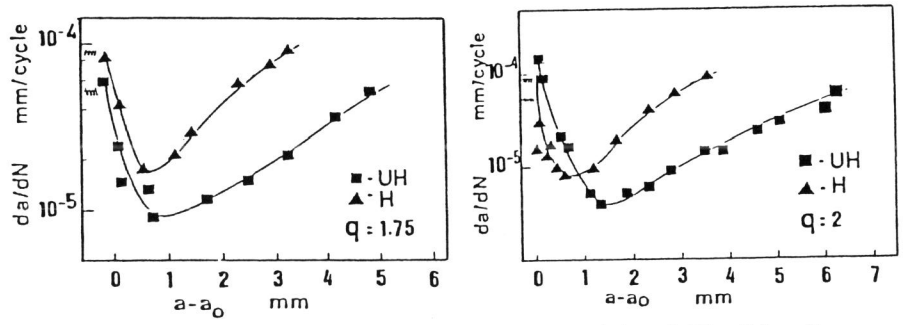

Fig. 2. Overload retardation curves: (a) q=1.75, (b) q=2. The symbols ⫻ ; // are the steady state FCPR for H and UH conditions, respectively

Figure 2 illustrates the typical retardation curves for different overload levels. Qualitatively, the delayed retardation curve profiles are preserved for the H and the UH conditions. Notice, the initial higher steady state FCPR of the H specimens as compared to the UH specimens. The main differences between the retardation curves of the both conditions are expressed in terms of two variations. Firstly, a relative curve shifting to the left occurred for the H material. In fact, $(a\text{-}a_o)_{min}$ (the incremental crack extension $(a\text{-}a_o)$ which corresponds to the minimum value, $(da/dN)_{min}$,

of the FCPR) actually yielded a lower value. Secondly, the overload affected crack length, $(a-a_o)_{acl}$, as determined from the retardation curves was found to be reduced for H specimens as compared to the UH material. These observed differences occurred consistently for the two values of q.

Figure 4 demonstrates results of UH material specimens tested at 296K for various q values. In order to obtain the same size of plastic zones, ΔK_{OL} was kept constant at 55 MPa·√m for the applied fatigue base line values, ΔK_{CA}, of 22, 33 and 44 MPa·√m. Notice again the typical curve profiles and the consistent relative shifting of $(a-a_o)_{min}$ with q. Low values of q increased this shifting, as indicated for ΔK_{CA} = 44 MPa·√m. In addition, the experimental $(a-a_o)_{acl}$ could be tracked with clear indication of reduced crack lengths for lower q values.

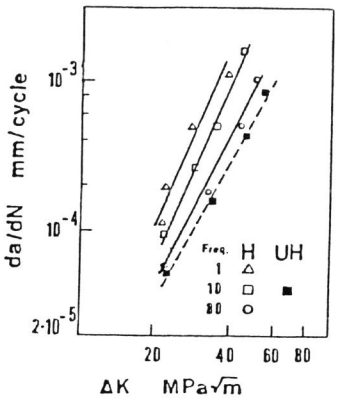

Fig. 3. Frequency effect in fatigue hydrogen charged AISI 304.

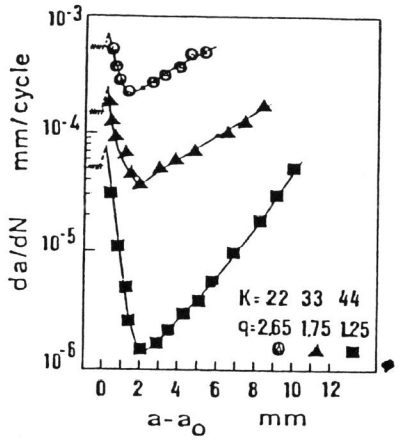

Fig. 4. Retardation curves after overload for constant plastic zone.

Table II summarizes some of the relevant results based on the current study.

TABLE II. Delayed Retardation Data in Unhydrogenated and Hydrogenated AISI 304.

Environment	q	$(a-a_o)_{min}$ mm	$(a-a_o)_{acl}$ (*) mm	N_D/N_{CA} (**)
UH	1.75	0.70	4.8	1.8
H	1.75	0.55	3.2	1.4
UH	2.0	1.30	6.3	4.0
H	2.0	0.70	3.5	2.7

* The overload affected crack length was determined from retardation curves
** The ratio between the fatigue cycles spent in the delayed affected plastic zone (N_D) and the cycles needed under constant amplitude without load interaction effects (N_{CA})

In Fig. 5 scanning electron fractography of a hydrogen charged specimen is illustrated. In this typical region (for $(a-a_o)$ = 0.1 mm) the crystallographic nature of the secondary micro-cracking is readily observed and was only typical to the combined interactive effects of cyclic crack propagatio accompanied by hydrogen charging. In contrast, striations were observed during fatigue in UH specimens. From acoustic emission (AE) tracking the following findings are summarized. Relatively to the steady-state fatigue crack extension without hydrogenation, the retardation region affected by hydrogenation is clearly associated with increased AE activity, accompanied by significant spectra differences.

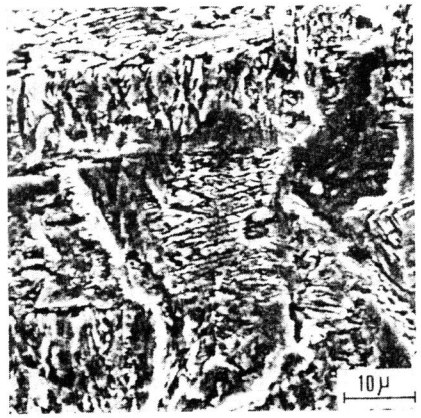

Fig. 5. Fracture appearance in H-charged specimen after overload at $a-a_o$=0.1 mm, q=2.5, and subsequent cycling at: ΔK=22 MPa·√m, f = 10 Hz.

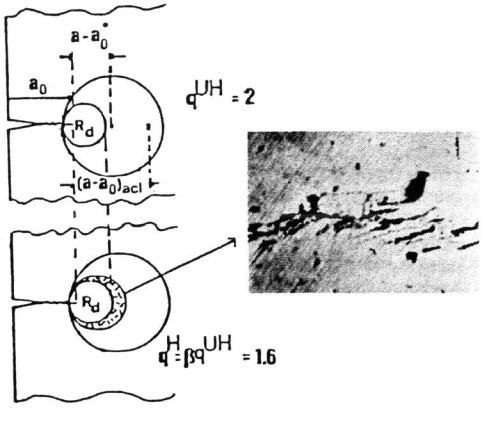

Fig. 6. Schematic illustration of single overload and subsequent fatigue run. Notice the modification of the hydrogenated dynamic plastic zone due to micro-cracking

DISCUSSION

Figure 3 demonstrates that the monotonic increasing tendency of the FCPR as obtained for UH material is well prserved for the H material under the specific experimental conditions. This behavior indicates that in the presence of hydrogen the FCP process is assisted by environment controlled fracture. In other words, the crack propagation is mainly mechanically controlled and further enhanced by the aggressive environment, while stress assisted dissolution process is negligable. As well illustrated, the extent to which the environment affects the FCPR, depends on the cycling loading frequency. The FCPR in terms of first approximation dependency functions can be expressed by the following constitutive relationships:

$$da/dN = A(\Delta K)^n \qquad (2)$$

for crack propagation caused by cyclic loading, or:

$$da/dt = \alpha da/dN = C(\Delta K)^m \qquad (3)$$

for crack propagation enhanced by environmental component, where A, C, n and m are constants and α is a modification factor which depends on the frequency and the applied waveform .

Referring to Fig. 2, it is seen that the phenomenological description of single overload effects in the environmentally exposed AISI 304 stainless steel, appeared very similar to the known influences which occur in UH specimens. For the sake of briefness, the discussion regarding the refined mechanisms which are responsible for shaping the retardation curve, i.e. residual stresses, blunting, closure or mismatching surface mechanisms, is skipped. However, the end result of all these mechanisms will be in altering the localized effective stress intensity factor amplitudes ΔK_{eff}. This localized term, namely, the effective mechanical driving force dominates the FCPR through the overload affected plastic zone. There have been attempts to estimate ΔK_{eff} by utilizing COD measurements or alternatively calculating the opening stress which reveal a similar FCPR retardation profile, due to load interaction (Lankford et al., 1976). In fact, Tokaji et al., (1983), have discussed some relevant features with respect to the retardation curve profile, mainly connected to the possible variation of the overload plastic zone caused by the environment.

Chanani (1978) and Wei et al., (1980) came to some different conclusions, since minor changes only, have been observed in the overload affected crack length in Al-alloy with environmental influences. In their studies, the decrease of N_D with the environment has been associated with higher FCPR, caused by the aggressive environmental factor,in contrast to variations in the overload plastic zone size. The current study intends to adopt a different approach, although the experimental evidences confirmed the tendencies, as determined by Chanani (1978), Wei et al., (1980) and Ranganathan et al., (1983). Experimentally, the role of hydrogenation on the overload affected plastic zone is readily observed as indicated by the typical retardation curves shown in Fig. 2. However it seems advisable to evaluate the hydrogenation effect by realizing the analogous results as determined for UH specimens as illustrated in Fig. 4. As mentioned already, the latter findings were obtained for various values of q by altering the subsequent fatigue base line amplitudes, and keeping the overload plastic zone size constant. Comparison between the two cases is really striking.

In the environmental case the typical variations of $(a\text{-}a_o)_{min}$ and the overload affected crack length $(a\text{-}a_o)_{acl}$ combine in fact two separate origins for crack extension rate influences. Firstly, the potential damage might be changed due to environmental degradation of the material, namely, a significant reduction of the fatigue resistance. Secondly, hydrogenation might modify the effective driving force caused by influences regarding the crack tip stress field, crack front geometry and residual stresses.

The current semi-empirical approach centers on the mechanical parameter. Namely, considering the mentioned analogy, the whole interactive effects are analysed by some modified value of q (increasing or decreasing) while the overload plastic enclave size is consistently preserved. Attributing the environmental effects only to the crack extension force as independent parameter, simplifies the analysis and provides some benefits in dealing with engineering design aspects. In other words, despite metallurgical and structural influences, which are well recognized, a mechanical description in terms of ΔK_{eff} is attempted as frequently applied in load interaction problems.

This modelling approach appears more adequate by realizing the dynamic plastic zone to be expressed by a modified value of q, namely $q^H = \beta q^{UH}$, where $\beta<1$ indicates an appropriate correction factor. For first order approximation, this can be obtained by increasing mechanically the value of K_{max} or the stress intensity amplitude range of the subsequent cycling (Fig. 6). Referring to Fig. 3, the following procedure was applied in order to calculate the correction factor β. First, da/dN, for H material, corresponding to the stress intensity factor range ΔK_{CA} = 22 MPa$\cdot\sqrt{m}$ was determined Then, for this value of crack velocity, the equivalent stress intensity factor range, ΔK_{eq} = 27 MPa$\cdot\sqrt{m}$, corresponding to the UH material was evaluated. Since we deal with constant overload plastic zone, it follows: $\beta = \Delta K_{CA}/\Delta K_{eq} \approx 0.8$.

Following this approach, the model of Willenborg et al., (1971) modified by Wei et al. (1980) can be applied. Here, a different variant is proposed, more inspired by Wheeler's (1972) concepts. The central issue is based on the invariant nature of the overload plastic zone with minor changes due to the aggressive environment.

According to the results for UH specimens, it is assumed that for a given constant overload plastic zone a typical $(a\text{-}a_o)^*$ exists (Fig. 6), indicating the characteristic distance where a maximum influential strength is developed. At $(a\text{-}a_o)^*$ the localized mechanical driving force for fatigue damage ΔK_{eff} is at the minimum for a wide range of fatigue amplitudes. Accordingly:

$$(a\text{-}a_o)_{min} = (a\text{-}a_o)^* - \Phi(R_d) \qquad (4)$$

here $\Phi(R_d)$ is an appropriate function which depends on the subsequent dynamic plastic zone.

For example, in case of UH specimens, for q = 2.5 (Fig. 4), the value of $(a\text{-}a_o)^*$ was found to be 2.8 mm, using the experimental value of $(a\text{-}a_o)_{min}$ and the simplified term for $\Phi(R_d) = R_d/2$. Other values of $(a\text{-}a_o)_{min}$ were calculated, using $(a\text{-}a_o)_{min} = 2.8$ mm. The obtained results are given in Table III, together with the corresponding experimentally determined values of $(a\text{-}a_o)_{min}$.

Table III: Experimental and calculated values for $(a\text{-}a_o)_{min}$

q	ΔK_{CA} MPa$\cdot\sqrt{m}$	$R_d/2$ mm	$(a\text{-}a_o)_{min}$ Exp.	$(a\text{-}a_o)_{min}$ Calc. from (4)
2.5	22	0.64	2.15	2.15
1.75	33	1.4	1.63	1.4
1.33	44	2.1	1.20	0.8

Modification of q actually changes the dynamic plastic zone embedded in the overload affected plastic zone which results in shifting of the retardation curve. From Eq. 4 the shifting of $(a\text{-}a_o)_{min}$ to the left is expressed by attributing higher $\Phi(R_d)$ value for reduced q. Accordingly, for the environmental case a modified q is considered by the mentioned modification factor β, expressing the role of the environmental effective stress intensity factor, ΔK^H_{eff}, which is given by:

$$\Delta K^H_{eff} = F(K_{OL};R;T_c;S_t;C_H) \qquad (5)$$

where: T_c and S_t are the tip constraint and the micro-structural factor respectively. Significant structural influences might be caused by austenite decomposition enhanced by deformation or by hydrogen charging. C_H is the hydrogen concentration level which dominates the intensified value of the subsequential fatigue amplitude.

A further extension of this approach can also incorporate the specific hydrogen/material charging parameters. Clearly, some variations in the interactive intensification factor are expected for different fugacity conditions which depend on the charging techniques (electrolytic or gaseous) surface conditions and related parameters. For example, in the present study electrolytic charging was performed with no poison, which caused significant reduction in hydrogen fugacity and resulted in intermediate degradation values.

The hydrogenation effects are well reflected in the fractographic evidence. In addition to secondery micro-cracking the crystallographic habits were observed in the damaged zone. Only in the case of intensive domination of fatigue damage, due to the high amplitude range of $\Delta K = 44$ Mpa$\cdot\sqrt{m}$, the typical striations in a continuum mode process were preserved, still accompanied with secondary cracking.

With respect to the AE activity, hydrogen clearly caused significant higher wave emissions. Moreover, in the H case good correlation exists between the crack extension rate and the AE activity, as tracked along the affected crack length. This complementary technique confirmed the localized damage process at the crack tip, as demonstrated and modelled schematically in Fig. 6. In spite of the complex aspects involved in interactive problems, the present comparative view might assist in expressing the environmental effects by a relatively simplified overload level factor.

CONCLUSIONS

(1) Environmental interactive effects, induced by hydrogen charging during steady state fatigue, resembled the phenomenological behavior as occurred in unhydrogenated material. However, over the entire region of applied stress intensity factor ranges, the environmental affected crack extension rates were higher than in case of the unhydrogenated material.
(2) Quantitatively, in the presence of hydrogen, the overload affected crack length and the number of cycles spent in the overload affected region are reduced, as compared to unhydrogenated specimens.
(3) The similar tendencies which were determined in unhydrogenated specimens, suggest a simplified analysis to account for the environmental influences in terms of an environmental interactive mechanical factor. Thus, evaluation of environmental susceptibility and life assessment with real fatigue spectra can be attempted.

ACKNOWLEDGMENT

The authors wish to thank Mr. M. Kupiec of the Nuclear Research Centre-Negev for experimental assistance during the present investigation.

REFERENCES

Bussiba A., H. Mathias and Y. Katz (1981). Fatigue crack propagation at low temperatures, Proc. Materials Eng. Conf. Haifa, Israel, Freund Publ. House, Tel-Aviv. 123-126.

Chanani G.R. (1978). ASTM STP 642, 51.

Katz Y., A. Bussiba and H Mathias (1981). The Influence of austenite stability on fatigue crack growth retardation. In: Materials, Experimentation and Design in Fatigue. Sherratt F., J.B. Sturgeon and R.A.E. Farnborough Eds. Westbury House, IPC Science and Technology Press, Guilford, Surrey. 147-158.

Katz Y., A. Bussiba and H. Mathias (1982). The role of induced phase transformation on fatigue processe in 304L. Proc. 4th European Conf. on Fracture (ECF4). Maurer K.L. and F.E. Matzer, Eds. EMAS U.K., 503-511.

Katz Y., A. Bussiba and H. Mathias (1984). Transitions in fatigue processes at low temperatures, Ad. Cryog. Eng. Mat., 30, 339-347.

Lankford J. Jr. and D.L. Davidson (1976). Fatigue crack tip pasticity associated with overloads and subsequent cycling. ASME J. Eng. Mater. Technol., 98. 17-23.

Mathias H., Y Katz. and S. Nadiv (1977). Post charging events in hydrogenated austenitic steels. Proc. 2nd. Int. Cong. on Hydrogen in Metals, Paris, Paper 2C-11. Pergamon Press, Paris.

Mathias H., Y. Katz and S. Nadiv (1978). Hydrogenation effects in austenitic stainless steels with different stability characteristics. Metal Sci., 12, 129-137.

Mathias H., Y Katz. and S. Nadiv (1982). Hydrogenation/gas release effects in austenitic steel: Quantitative study. In: Metal-Hydrogen System, Veziroglu T.N. Ed., Pergamon Press, Oxford 225-249.

Ranganathan N. and J. Petit (1983). Quantitative measurement in the plastic zone caused by a single overload in air and vacuum. Fatigue Mechanism: Advances in Quantitative Measurement of Physical Damage, ASTM STP 811, 464-484.

Tokaji K., Z. Ando, T. Imai and T. Kojima (1983). Fatigue crack retardation of high strength steel in saltwater. ASME J. Eng. Mater. Technol., 105, 88-92.

Wei R.P., N.E. Fanelli, K.D. Unangst and T.T. Shih (1980) Fatigue crack growth response following a high-load excursion in 2219-T851 aluminum alloy. ASME J. Eng. Mater. Technol., 102, 280-292.

Wheeler O.E (1972). Spectrum loading and crack growth. ASME J. Basic Eng. 94, 181-186.

Willenborg J.D., R.M. Engle and H.A Wood (1971). A crack growth retardation model using an effective stress concept. AFFDL-TM-71-1-FEB.